Study of evolution of three-dimensional porous structure in zeolite-templated carbons

Madi Arsakay[1,2], Boyuan Shen[1,3]*, Xiao Chen[4], Hao Xiong[4], Korlan Duisenova[1,2], Alisher Fatkhulloev[1,2], Carola Vorndran[5], Guangwu Yang[6], Bayrammuhammet Annageldyyev[8], Sun Hwa Lee[1], Won Kyung Seong[1], Matthias Thommes[5], Fei Wei[4], Rodney S. Ruoff[1,2,7,8]**

[1]Center for Multidimensional Carbon Materials (CMCM), Institute for Basic Science (IBS), Ulsan 44919, Republic of Korea.

[2]Department of Chemistry, Ulsan National Institute of Science and Technology (UNIST), Ulsan 44919, Republic of Korea

[3]Institute of Functional Nano & Soft Materials (FUNSOM), Jiangsu Key Laboratory for Carbon Based Functional Materials & Devices, Joint International Research Laboratory of Carbon-Based Functional Materials and Devices, Soochow University, 199 Ren'ai Road, Suzhou, 215123, Jiangsu, China.

[4]Beijing Key Laboratory of Green Chemical Reaction Engineering and Technology, Department of Chemical Engineering, Tsinghua University, Beijing 100084, China.

[5]Institute of Separation Science and Technology, Department of Chemical and Biological Engineering, Friedrich-Alexander-Universität Erlangen-Nürnberg, Germany.

[6]School of Material Science and Engineering, China University of Petroleum (East China), Qingdao, 266580, China.

[7]Department of Materials Science and Engineering, Ulsan National Institute of Science and Technology (UNIST), Ulsan 44919, Republic of Korea.

[8]School of Energy and Chemical Engineering, Ulsan National Institute of Science and Technology (UNIST), Ulsan 44919, Republic of Korea.

*Correspondence: byshen@suda.edu.cn

**Correspondence: ruofflab@gmail.com

Summary

The atomic-scale and near-atomic-scale local structures during zeolite-templated carbon (ZTC) growth are not well understood. Our study provides insights into the structural evolution from the early to later stages, and finally, the completed stages of growth (i.e., carbon deposition inside the zeolite pores) of Ca-exchanged FAU zeolite-templated carbon using acetylene as a

carbon source, through integrated differential phase contrast (iDPC) STEM. Furthermore, the combination of CO_2 and Ar adsorption techniques provides a full pore size distribution and provides values for the inner and outer surface areas and volumes of the hollow carbon structure. These findings can help to better understand the structure of ZTCs at the atomic and near-atomic levels, which can be leveraged to enhance ZTC performance in existing applications and potentially enable their use in new applications.

Keywords

zeolite, zeolite templated carbon, iDPC-STEM, atomic resolution, surface area, gas adsorption, carbon.

Introduction

Trivalently-bonded carbon (TBC*)* is the basic unit of a variety of carbon allotropes including fullerenes,[1] carbon nanotubes,[2] graphene,[3] and various three-dimensional (3D) porous carbon structures.[4-7] Different 3D architectures of porous carbons composed of TBC have attracted wide interest for basic science studies and potential use in catalysis, adsorption, mechanics, electronics, and energy storage, among others.[8-14] For example, schwarzites[6] contain network pores with negative-curvature surfaces and an open topology. There are (in principle) an infinite variety of schwarzites, and since they are a sub-class of all porous carbons composed of TBC, the structure space in terms of even further variety is even larger. In short, an infinite number of different unit cells that periodically repeat can be formed at least in principle. In addition to computational modeling, what experimental approaches have been or could be used to deepen our understanding of this class of structures?

One is “bottom-up” synthesis that requires the accurate control of five-, six- or seven-membered rings to form negative-curvature surfaces, and exciting progress is being made.[15] Another is “top-down” synthesis by templating the carbon product using existing porous and periodic (crystalline) solids, such as zeolites,[16-25] yielding “zeolite-templated carbon” (ZTC). The wide variety of zeolites[26] suggests that a wide variety of ZTCs can likely be generated.[16] Removal of the zeolite template after depositing carbon inside its pores yields the ZTC. The topology of this ZTC will depend on the structure of zeolite template, while the properties of this ZTC benefit from both the graphene-like surfaces and periodic micropores. (Here, ZTC is “the templated carbon with zeolite removed” and C@FAU is “the templated carbon with the zeolite still present.”)

FAU is a naturally occurring aluminosilicate zeolite also synthesized in large scale for commercial applications, and that has been used to synthesize certain ZTCs.[16-25] When metal ions, such as La^{3+} and Ca^{2+}, were introduced by ion exchange of some of the Na^{+} ions conventionally present in FAU, it was reported that acetylene and ethylene could be carbonized inside the zeolite pores at a relatively low temperature compared to the earlier syntheses of ZTCs.[19] A carbon "replica" of the ordered micropores in this La- or Ca- FAU zeolite was reported to have high surface area, low density, high rigidity, good stability and relatively high electrical conductivity.[19]

Real ZTCs are not *perfectly* periodic, since there is disorder on the local (i.e., atomic) scale and it seems that not all the zeolite channels are perfectly filled by TBC.[19,27] Note that ZTCs are typically analyzed by powder X-ray diffraction (PXRD), gas adsorption isotherms, Raman spectroscopy, and solid state nuclear magnetic resonance (SSNMR); these have not provided high-spatial-resolution information of atomic-scale and near atomic-scale local structures (we note that multidimensional SS-NMR might eventually provide such information but are not aware of any such studies on ZTCs; indeed we are planning such studies in the future). Thus, the evolution of the growth, from the initial to the final stages, of ZTCs and other porous carbons is not yet really well understood, with recent attempts reported about beta zeolite and ethylene as a carbon precursor and FAU zeolite (sodium counterion) and acetylene as a carbon precursor (carbon deposition done at 600°C), FAU zeolite (proton counterion) and ethylene as a carbon source at 680°C.[28-30] Our study here provides insights into the structure from the early to the latter, and final, stages of growth (carbon deposition inside the zeolite pores) of the Ca-exchanged FAU zeolite templated carbon using acetylene as a carbon source.

(Scanning) transmission electron microscopy, (S)TEM, has a high spatial resolution and can resolve atoms and bonds including in periodic structures.[31-33] Zeolites, and the carbons grown inside its channels, are composed of low atomic number elements and are thus beam-sensitive, which limits the *sample stability* and also *spatial resolution* and *signal-to-noise ratio* of the (S)TEM images acquired with standard STEM modes. Recently, *integrated differential phase contrast* (iDPC) STEM has been introduced,[34-36] and applied to atomic-scale imaging of various porous materials including zeolites[37-39] and metal-organic frameworks,[40] given its low electron dose, high *signal-to-noise ratio* and other favorable attributes. Indeed, small and individual aromatic molecules confined in zeolites have been imaged with excellent contrast.[41,42] We report here how the iDPC-STEM can be applied for studying the ZTC structures during the initial-through-final stages of carbon growth.

We find that the real-space imaging of the FAU template and ZTCs by the iDPC-STEM shows an ultrahigh resolution and good signal-to-noise ratio and provides details about local structures. Combining the iDPC-STEM images with other characterization results, the ZTC product is found to have a near-periodic network and hollow structure of TBCs that "replicates" the FAU template. We report on the evolution of carbon and also of carbon structure in the FAU zeolite as a function of time by interrupting growth before it is complete. In addition to atomic-scale iDPC-

STEM imaging, we report (as far as we are aware, for the first time) the volume and surface area of the "inside" and "outside" surfaces of a ZTC (defined as V1, V2 and S1, S2, respectively) obtained from the gas adsorption isotherm (CO_2 273 K and Ar 87 K) measurements. That is, prior to removal of the zeolite by etching it away, S1 and V1 are the "inside surface and volume". After removal of the zeolite, S2 and V2 are the "outside surface and volume". We report our study in detail below.

Results and Discussion

STEM images of FAU template

Figure 1A and Figure S1 show the structural model of FAU zeolite. The FAU framework contains 0.74-nm *channels* and 1.12-nm *cages* with each cage connected with four other cages by "short neck" channels as shown in Figure 1B. Such a network of channels and cages comprise the space for carbon deposition and thus determines the topology of the ZTC structure if the templating works well. Several different models of TBC structures based on the FAU zeolite template have been reported.[12,16,18,19,21,23,25] We have chosen to use the model reported by K. Kim, et al., which shows the electron-density map of C atoms obtained by single-crystal X-ray diffraction data (Figure 1C).[19] Note that the real ZTC structure was reported to have high static disorder, especially at "short neck" channels, where the electron densities were reported to be too crowded to assign C-C bonding. This reported model indicates that the real ZTC structure is hollow, that is, the C atoms are formed into a network that replicates the porous FAU template along its curved inner surface (at least in the supercage region).[19]

We used annular dark field (ADF) STEM and iDPC-STEM to study the crystal shapes and atomic structure of the FAU template; we chose to focus on FAU zeolite with Ca^{2+} ions (Ca-FAU) that are inserted by ion exchange. Figure 1E shows the [111] projection of the FAU lattice acquired from the red frame in Figure 1D. The FAU channels are imaged in this projection. Figure 1F gives the comparison of a magnified iDPC-STEM image and the structural model and this shows that the Ca-FAU channel system is consistent with the model. Atomic imaging of the FAU lattice was achieved from the [110] direction (Figure 1G-I). Figure 1H is an atomic-resolution iDPC-STEM image of the [110] projection of Ca-FAU, acquired from the thin region at the crystal corner (the red frame in Figure 1G). Compared to the image of H-FAU without Ca^{2+} ions (there are still some H^+ and Na^+ ions, see Figure S2) where the channels are nearly empty, there are obvious additional contrasts inside the channels of the Ca-FAU sample. Elemental mapping (Figure S3) of H-FAU and Ca-FAU by energy dispersive spectroscopy (EDS) indicates that these additional contrasts in the channels should be the Ca^{2+} ions connected to acid sites (Al sites) and exposed in channels (the "contrasts" of H^+ and Na^+ ions were too low to be observed; note that Na signal was detected by EDS, see Figure S3. EDS cannot detect H).

Figure 1I includes the magnified iDPC-STEM images at the regions with empty channels and Ca^{2+}-filled channels, respectively. The atomic positions of **T** (Si or Al atoms) and **O** (O atom) sites can be identified in the magnified images, which are highly consistent with the structural model and thus simulated image in Figure S4. To further test this assigned atomic structure, we applied profile analysis to the iDPC-STEM image. Figure 1J shows two intensity profiles obtained from the regions that are marked by the red and blue frames in Figure 1I. In the 'red' profile, we can identify two peaks for **T** (Si or Al) atom columns and the middle small peak for the **O** atom column. The peaks in the 'blue' profiles represent four projected positions of **O** atom columns. Thus, the **T** and **O** sites can be well resolved by the iDPC-STEM imaging, which, to the best of our knowledge, has not been reported for the FAU zeolite. Such atomic imaging of the Ca-FAU lent us confidence to further study the growth from *early* to *middle* to *final* stages of the carbons "templated" by the Ca-FAU.

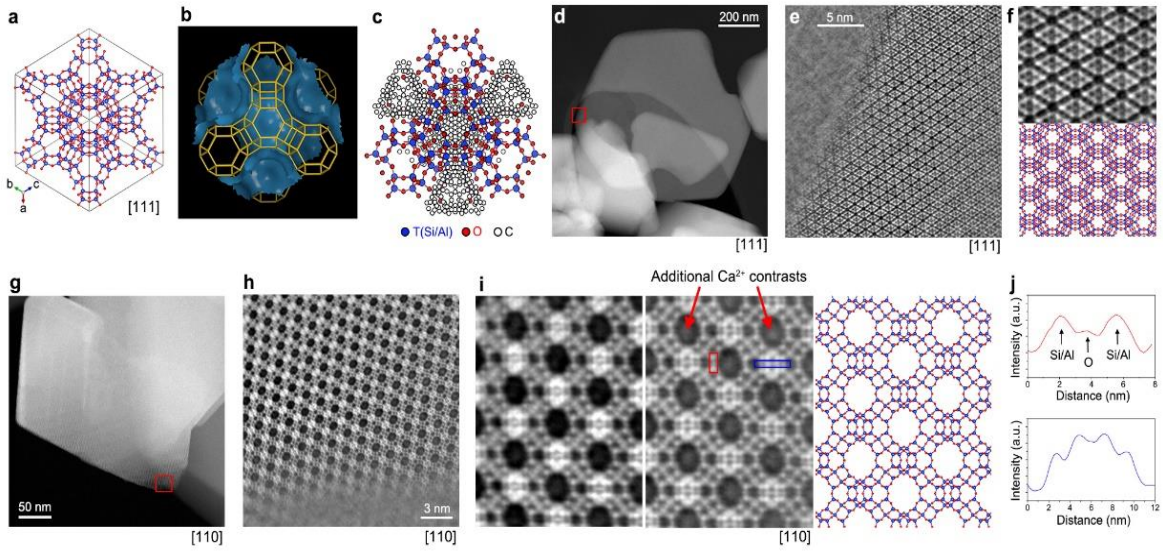

Figure 1. STEM images of FAU template
(A) Structural model of FAU zeolite viewed from the [111] direction.
(B) Channel system of the FAU zeolite.
(C) Probable structural model of C@FAU sample.
(D) ADF-STEM image of FAU zeolite viewed from the [111] direction.
(E) iDPC-STEM image of FAU zeolite obtained from the red box in (D).
(F) Comparison between the magnified iDPC-STEM image and the structural model viewed from the [111] direction.
(G) ADF-STEM image of the FAU zeolite viewed from the [110] direction.
(H) iDPC-STEM image of the FAU zeolite obtained from the red box in (G).
(I) Comparison between the magnified iDPC-STEM images (with and without Ca^{2+} ions) and the structural model viewed from the [110] direction.
(J) Profile analysis of the magnified iDPC-STEM image obtained from the red and blue boxes in (I).

ZTC synthesis and characterization

The ZTCs were synthesized at 450°C and 700 torr using acetylene (20 sccm) mixed with Ar (80 sccm). A parametric study of temperature and pressure was "optimized" as shown in Figure S5. FAU templates with Ca^{2+}, Mg^{2+}, La^{3+}, and Y^{3+} were prepared by ion exchange (see Methods). Figure 2A shows the weight ratio of carbon-to-zeolite with different reaction times and the different metal ions. The time of exposure to acetylene was varied, and the acetylene flow was turned off at a given time (but Ar was left on) following which the samples were heated at 850°C for 2h.[43] Thermogravimetric analysis (TGA) is shown in Figure S6. The Ca^{2+}, Mg^{2+}, La^{3+}, and Y^{3+}-exchanged FAU templates show a similar trend of *carbon content vs exposure to acetylene time.* The carbon content (the weight ratio of carbon-to-zeolite) plateaus at a value of about 0.30 for these four FAU templates. We henceforth focus on results for the Ca-FAU; note that some results for Mg^{2+}, La^{3+}, and Y^{3+} are shown in the Supporting Information (Figure S7-S9). Since these supporting results indicate a similar ZTC structure for different metal ions, the study on the ZTCs from Ca-FAU template is perhaps representative of all samples that we have prepared (but further study is indicated).

Figure 2B shows the PXRD results of Ca-FAU and ZTC, and the sharp peak at 6.5° shows the replication of the FAU (111) planes. ^{13}C SSNMR and Raman spectroscopy indicate the presence of TBC in the ZTC. The single peak at 120-130 ppm in the ^{13}C SSNMR spectrum (Figure 2C) is from TBCs. The G-band and D-band in the Raman spectrum (Figure 2D) can be interpreted as due to TBC networks with C-H defects.[21] Figure 2E shows a scanning electron microscope (SEM) image of the ZTCs after removing the Ca-FAU templates, which is similar to those of the FAU particles (Figure S10). The ZTCs were also imaged by ADF-STEM (Figure 2F). The magnified high-resolution TEM image in Figure 2G shows the curved layers in networks at the edge of porous ZTC.

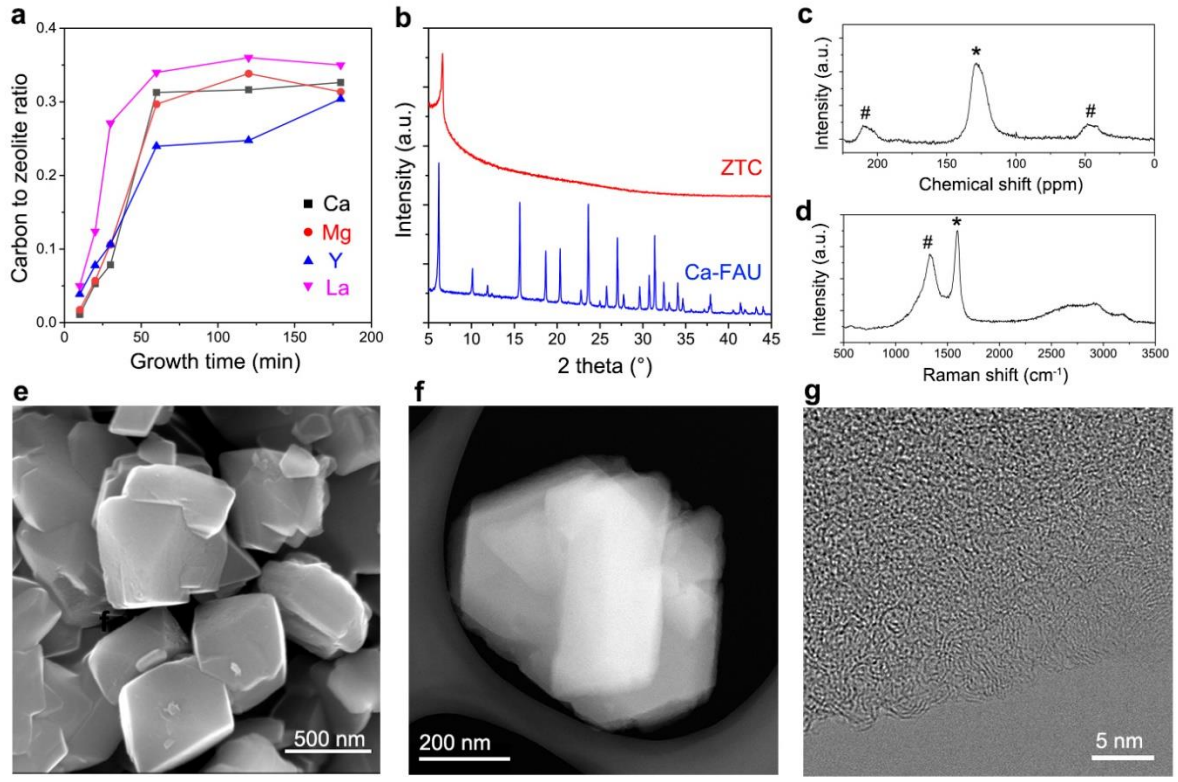

Figure 2. ZTC synthesis and characterization. All results in (B) – (G) are about the Ca-FAU zeolite, and ZTC is (nominally) carbon only, that is, the zeolite has been removed

(A) Carbon content (carbon-to-zeolite mass ratio) for different growth times as measured by TGA.
(B) PXRD results of Ca-FAU zeolite and the ZTC.
(C) ^{13}C SSNMR spectrum of the ZTC. Asterisk shows the chemical shift at 120-130 ppm indicative of TBC. Hashes indicate the spinning sidebands.
(D) Raman spectrum of ZTC. Asterisk and hash indicate the G-band and D-band, respectively.
(E) SEM image of the ZTC.
(F) ADF-STEM image of the ZTC.
(G) Magnified high-resolution TEM image of the ZTC.

Adsorption measurements of ZTC

We then used gas adsorption isotherms to study the microporous structure of ZTC in detail. According to the model based on the electron-density map of C atoms,[19] the negative curvature of a hollow carbon structure should be expressed in two different kinds of pore widths in the whole pore size distribution, which correspond to the pore volumes inside and outside the hollow carbon structure, defined as V1 and V2, respectively. For this we applied Ar adsorption at 87K as

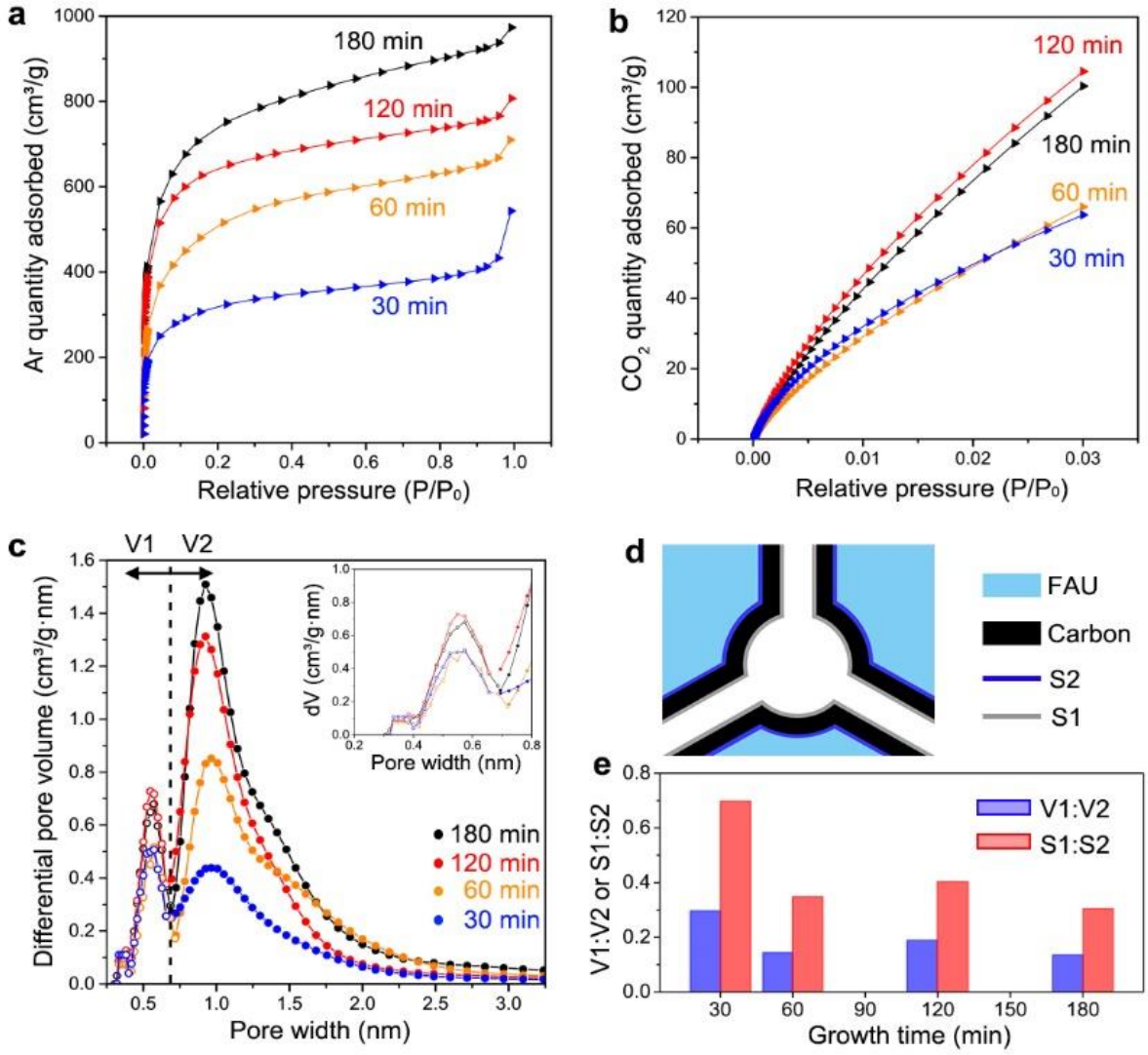

Figure 3. Adsorption measurements of ZTC

(A) Ar (87 K) adsorption isotherms of the ZTC samples with different growth times.

(B) CO_2 (273 K) adsorption isotherms of the ZTC samples with different growth times.

(C) Pore distributions of the ZTC samples with different growth times obtained from the combination of Ar (using a dedicated QSDFT slit pore kernel) and CO_2 (using a dedicated NLDFT slit pore kernel) adsorption isotherms (bullet points and circles, respectively). V1 and V2 represent the pore volumes as described in the text.

(D) Schematic model to define the inner and outer surfaces (S1 and S2) of hollow ZTC structure.

(E) Change of V1:V2 and S1:S2 ratios of the ZTC samples with growth time.

well as CO_2 adsorption at 273 K. CO_2 adsorption at 273 K is a standard method for the assessment of carbon nanopores of width < 1 nm and the combination of Ar and CO_2 adsorption allows one to obtain the complete pore volume/size distribution ranging from ultramicropores to meso/macropores.

Figure 3A shows the Ar adsorption isotherms of the ZTC samples after etching that were obtained by different times of exposure to acetylene (different growth times). They were used to detect the pores with a width > 0.7 nm, which contribute most of the pore volume and surface area in these ZTCs. The Brunauer-Emmett-Teller (BET) areas obtained by Ar adsorption isotherms are 990, 1500, 2050, and 2280 m^2/g for the 30-, 60-, 120-, and 180-min samples, respectively. It should be noted that these BET areas only represent apparent surface areas, because the BET theory cannot be applied in a strict sense on adsorption data obtained on microporous materials.[44] The increasing BET area with growth time indicates that the microporous structure was gradually formed during the growth process. As for pores < 1 nm, the CO_2 adsorption isotherms were used to supplement the pore size distribution in the nanopore region (Figure 3B). In these isotherms, the amount of CO_2 adsorbed in the 30- and 60-min samples are nearly identical, which correspond to the space inside the hollow ZTC, while more CO_2 was adsorbed in the 120- and 180-min samples.

Combining the Ar and CO_2 adsorption results, as indicated above, we calculated, for the different samples, the pore size distributions in the range from ultramicropores to narrow mesopores by applying advanced methods based on statistical mechanics, i.e., the non-local density functional theory (NLDFT) method for CO_2 and quenched solid density functional theory (QSDFT, which takes into account surface roughness) for the Ar data, assuming in both cases a slit pore model.[45,46] With regard to this, it should be noted that the calculated pore size is strongly depending on the chosen pore model, i.e., here we apply for simplicity a slit pore model, which may underestimate the true pore width but still is capable of producing the correct character of the pore size distribution curve, i.e., here a bimodal distribution. The circular and round data points in Figure 3C were extracted from the Ar and CO_2 adsorption, respectively, and then combined to indicate the V1 and V2 that are defined on both sides of the dashed line. The pore volume at the pore widths of about 1 nm is naturally the volume generated after etching the zeolite (that is, V2, nearly consistent with the previous results[19]). The pore volume at the pore widths of about 0.6 nm indicates the inner space of the ZTC (that is, V1), which, although CO_2 adsorption was done before,[27,29] has not been previously reported for perhaps similar ZTC samples. We present a model in Figure 3D to define the V1 and V2, as well as the corresponding S1 and S2 of this type of carbon structure. S1 is the accessible surface prior to etching the zeolite, that is, the inner surface of the ZTC. S2 is the other surface generated when we etch the zeolite away, that is, the outer surface of the ZTC.

Based on the cumulative surface area and pore volume in Figure S11 calculated based on the CO_2 and Ar adsorption isotherms shown in Figure 3A and 3B, we can assign the S1 (V1) and S2 (V2) with the pore width at 0.7 nm as the dividing line. The values of V1, V2, S1, and S2 for

these four samples are given in Table S1. V1 and S1 were obtained from the cumulative volume and surface area curves (Figure S12) with pore width ranging from 0 to 0.7 nm, while V2 and S2 were obtained from those with pore width ranging from 0.7 to 5.0 nm (reaching the maximum of volume and surface area). For the 180 min sample, V1 and V2 are 0.14 and 0.99 cm^3/g, and S1 and S2 are 500 and 1640 m^2/g. The ratios of V1:V2 and S1:S2 in the different samples are given in Figure 3E. The changes of these ratios and pore size distribution can help to understand the structural evolution of the ZTCs during the carbon deposition. At 30 min, some of the FAU cages were filled by the hollow carbon segments, but the rigid connections (necks) between the cages were not yet well formed. Therefore, when we etch the zeolite away, the pores with about 1 nm sizes (the outer space of these ZTCs) collapsed, while some of the pores with about 0.6 nm sizes (the inner space of the hollow ZTCs) remained. For 60 min, the carbon content still increased (the carbon-to-zeolite ratio, as shown in Figure 2A) accompanied by improved integrity of connections, so that more V1 was available and the V2 does not change. After further growth from 60 to 180 min, the carbon-to-zeolite ratio reached the plateaus at about 0.3, the network of ZTC was more rigid and the V1 and V2 reached their maximum values. The real-space imaging of carbon deposition in Figure 4 further supports this picture.

Due to their high surface areas, chemical composition, and chemical and thermal stability, ZTCs, including derived from FAU, were tested in adsorption, hydrogen storage, methane storage, and carbon dioxide capture[47]. However, the effect of S1, V1, S2, and V2 in these studies is not well understood, and their values and ratios may play crucial roles. As the number of closed strut moieties, as referred to by Choi et al.,[27] increases, the S1 and V1 values also rise. In an ideal case, where all pores are occupied by interconnected CLMs, the final structure will consist of two interpenetrating but non-connected surfaces. These structures can exhibit interesting mechanical, electronic, catalytic, battery, and gas sorption properties.

iDPC-STEM measurements of C@Ca-FAU

As mentioned, the iDPC-STEM enables atomic-imaging of beam-sensitive and light-element atoms, molecules, and structures. Thus, in addition to imaging the Ca-FAU, we could also observe the growth and distribution of carbon species in it. Figure 4A-D show four iDPC-STEM images of the [110] projections of different "C@Ca-FAU" samples made with the reaction times

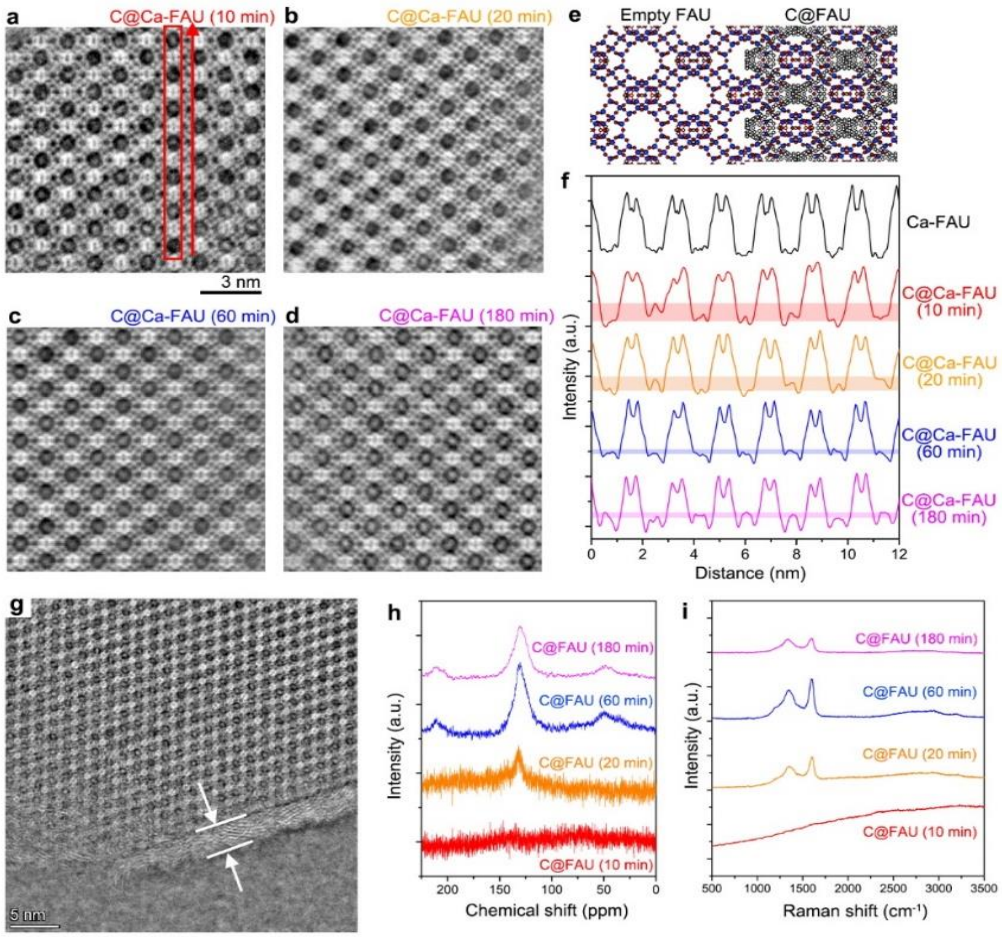

Figure 4. Structural analysis of C@Ca-FAU with different growth time

(A-D) iDPC-STEM images of C@Ca-FAU samples with different growth times.

(E) Structural model of empty FAU and C@FAU (note: not specifically Ca-FAU).

(F) Profile analysis of iDPC-STEM images of empty Ca-FAU and C@Ca-FAU samples for different growth times. The profile width and direction in (B-D) are the same as those shown in the red box and red arrow in (A). The colored horizontal bands for 10-, 20-, 60-, and 180-min C@FAU products show the range (the "spread") of C peak heights (obtained in the channels). Notice that this spread is much smaller in the 60- and 180-min samples.

(G) iDPC-STEM image of the 180-min C@FAU sample showing the surface carbons. (H) ^{13}C SSNMR spectra of C@FAU samples with different growth times.

(I) Raman spectra of the C@FAU samples with different growth times.

of 10, 20, 60, and 180 min, respectively. Regions in the channels with significantly different contrast compared to the empty Ca-FAU sample (Figure 1I) are evident. These regions were confirmed to contain carbon species as shown by EDS (Figure S12 and S13; and please note the other characterizations given in Figure 4). The structural evolution of carbon network from

partial to possible complete filling of these Ca-FAU channels could be assessed from these four iDPC-STEM images (typically 4 or 5 images were obtained for each sample—the images shown in 4a-d are representative).

As shown in Figure 4A and 4B, some channels are partially filled by carbons and others are nearly empty. The carbon contrasts in the Ca-FAU channels of the samples made by 10-minute or 20-minute exposures to acetylene vary over a wide range, indicating that a complete network has not been formed (note that the *carbon content* is about 0.05), and that some channels have more carbon than others. The convergent semi-angle of 15 mrad corresponds to a depth of focus of 18 nm, which means that all the "carbon information" for 18 nm along these channels is contained in these images. The carbon content of the 60 and 180 min (*exposure to acetylene*) samples is about 0.30—as carbon values plateau, most of the FAU channels are filled by a TBC network (but they are not fully templated to reach ratio of 0.62-0.68 ZTC g/zeolite g, as seen from modelling);[27,29] as shown in Figure 4C and d, the carbons are more uniformly distributed and show high contrast in all channels. Figure 4E gives the structural models of empty FAU and C@FAU viewed from the [110] projection. As mentioned above, the model of C@FAU sample is based on the single-crystal X-ray diffraction data reported by K. Kim, et al.,[19] as shown in Figure 1C. There is obvious contrast (representing C atoms) appearing in each channel from this [110] projection after carbon deposition, which is consistent with our imaging results.

Profile analysis was used to address the change of carbon contrast in different regions and, thus, the structural evolution of the carbon network. The profiles in Figure 4F were obtained in the same area and direction as marked by the red box and red arrow in Figure 4A. The valleys in these profiles indicate the Ca-FAU channels, while the small peaks in these valleys indicate the carbons. The height of the carbon peak is positively correlated to the quantity of carbon atoms in each channel. In the profile of the pristine Ca-FAU sample, we can hardly observe a carbon peak. For the 10- and 20-min samples, the peak intensities (heights) show the breadth of the variation in carbon contrasts (marked by the translucent color bands). The carbon peaks from the 60- and 180-min samples are all nearly the same height and this value is usually higher than those of the 10- and 20-min samples. Then, as shown in Figure 4G, there is a 3-nm thick layer of carbon (it might contain some H) deposited on the surface in the 180-min sample, but this was not found in the 60-min sample (Figure S14). It was also confirmed by the Ar (87 K) adsorption results in Figure S15. Such surface carbon layer evidently blocks the Ar adsorption into the pores and channels. We noticed that this ~3-nm thick layer can be removed during the etching (removal) of zeolite template, since a BET surface area of up to 2280 m^2/g was then obtained.

Extra characterization

The ^{13}C SSNMR spectra for these C@Ca-FAU samples (with different growth times) in Figure 4H show one peak at 120-130 ppm (indicative of TBC) for the 20-, 60- and 180-min samples (no signal for the 10-min sample due to the too small quantity of carbons). The signal-to-noise ratio of this TBC peak increased as a function of growth time. The consistent G-band and D-band in

the Raman spectra of these three samples in Figure 4I also shows the formation of a TBC-extended structure. These results show that the ZTC has experienced a process from distributed early-stage growth to uniform filling at the latter stage. The carbon atoms of decomposed acetylenes originally form TBC segments that are distributed (perhaps somewhat randomly) in FAU channels. Such segments then further grow to connect into rigid networks yielding finally a (not full) replication of the FAU framework. When these FAU channels are being filled by carbons, the newly added carbons are trivalently-bonded.

The X-ray photoelectron spectra (XPS) survey spectrum in Figure S16 shows only carbon and oxygen present. The C1s spectrum exhibits mainly C-C/C=C (274.79 eV) bond and negligible amount of C-O (286.42 eV) and C=O (287.19 eV) bonds. It means that the ZTC is composed mainly of carbon.

We suggest: The C atoms obtained from the decomposition of acetylene are deposited in each channel (pore) at a range of rates (rather than uniformly—at least in the initial stages of growth). This non-uniform distribution of carbon atoms in different channels (for the 10- and 20-min exposures to acetylene) might be contributed by the non-uniform distribution of Ca^{2+} ions that is shown in Figure 1E. Also, there ought to be a stochastic aspect in terms of how acetylene molecules enter and diffuse along channels (if they do diffuse—perhaps they dissociate "quickly" and other C-containing species diffuse)—that is, it would be surprising and also unexpected if the rate of entry of acetylene into each channel at its pore entrance(s), and subsequent decomposition rates, were identical for all channels in an FAU particle. For longer exposure times to acetylene, such as 60 or 180 min, the channels (pores) are evidently further filled, and the growing carbon fragments are connected to form a 3D porous network. This picture agrees with the progression of carbon growth from the fragments in each channel to the hollow and porous structures that we deduced from the results of gas adsorption in Figure 3.

Methods

Synthesis of ZTC

The FAU zeolite template with a Si/Al ratio of 5.1 was purchased from Alfa Aesar. The ion exchange was performed with 1M aqueous solution of metal salts, including $CaCl_2$, $LaCl_3$, $MgCl_2$ and $Y(Ac)_3$, at 80°C for 1h. 3.3g of FAU zeolite and 100 ml of 1M solution was used. The ion exchange procedure was done three times. The FAU zeolite template (300-500mg) was placed in a vertical chemical vapor deposition tube and the tube was pumped out until 10^{-3} torr. The tube was then 'backfilled' with dry Ar(g) at a rate of 1000 sccm up to 700 torr, at which time heating until 450°C at a ramp rate of 5°C/min was started. Once the temperature reached 450 °C it was held at that temperature for 30 min and then the Ar flow rate was changed to 80 sccm and acetylene was introduced at a rate of 20 sccm for different times (for example: 10 min, 20 min, 30 min, 60 min, 120 min, 180 min) at 450°C. At the end of these time periods the gases were

evacuated, and the tube was backfilled with Ar with flow rate of 1000 sccm up to 700 torr, and heating until 850 °C was initiated. Once T reached 850°C it was held at this T for 30 min (making sure T is stable at this value) and then maintained for 2 h more at this T. After that, the system was cooled down to room temperate naturally and the C@FAU samples were then collected. ZTC samples were obtained after removing the FAU template in a 0.3 M HF/0.15 M HCl solution.

High-resolution (S)TEM imaging

All the (S)TEM imaging by different modes was carried out using a Cs-corrected STEM (FEI Titan Cubed Themis G2 300) operated at 300 kV. For the iDPC-STEM imaging, the convergence semi-angle is 15 mrad, and the collection angle is 4-22 mrad. The beam current is lower than 0.5 pA (and limited by the precision of the Faraday cup) with a dwell time of 32 μs and a pixel size of 0.3555×0.3555 $Å^2$. For the ADF-STEM imaging, the convergence semi-angle is 15 mrad, the collection angle is 17-102 mrad, and the beam current is 338 pA with a dwell time of 8 μs and a pixel size of 32.05×32.05 $Å^2$. For the high-resolution TEM, a BM-Ceta detector was used with a pixel size of 39.35×39.35 $Å^2$. The EDS elemental mapping was also carried out using this Cs-corrected STEM; the beam current for the EDS is 247 pA with a dwell time of 24 μs and a pixel size of 64.11×64.11 $Å^2$. The EDS data were integrated using the Velox software. Multi-polynomial and Brown-Powell models were employed to correct background and quantify the EDS data. The image simulations for the iDPC-STEM images were carried out based on the multi-slice method.[48,49] The parameters for simulations were selected to be the same as those in our imaging experiments. The four-segment detectors generated four images, which were firstly blurred with a Gaussian blur to account for incoherency of the source. And, the resulting images can be further processed to obtain the iDPC image, according to the integration step described by I. Lazić, et al.[35]

Other characterizations

The SEM images were collected using FEI Verios 460 SEM with an EDS accessory (Octane Elect EDS System) and Magellan 400 at 1.0-2.0 kV.

The TGA to measure carbon content was done with a TA Instrument Q 500 analyzer using a high-temperature platinum pan and heating to 900°C at a rate of 10°C min^{-1} under an air stream.

The PXRD patterns were collected using a Rigaku Smartlab diffractometer, operated at 40 kV and 200 mA in the 2theta range of 5 to 90° using Cu-Kα radiation (λ= 1.5418 Å).

The Raman spectroscopy was done using a WITec GmbH Raman microscope with the power of 1 mW and the laser wavelength of 532 nm.

The ^{13}C SSNMR spectra were recorded using a Bruker 500 MHz SSNMR spectrometer at room temperature.

The Ar (87K) and CO_2 (273K) adsorption isotherms were obtained using Micromeritics ASAP 2020. Zeolite and carbon samples were degassed following preloaded procedures in Micromeritics ASAP 2020, at 350°C for 480 minutes and 180°C for 200 minutes with ramp rate of 10.0°C/min, respectively. The Ar data were analyzed to obtain the BET surface area and relative pressure range of 0.001 to 0.1 was used. Ar adsorption data was analyzed using a dedicated QSDFT slit pore model, CO_2 adsorption was analyzed using a NLDFT slit pore model using VersaWin software by QuantaTec, Anton Paar.

A VarioEL cube element analyzer was used to determine the content of C, H, O elements in different samples. Under high temperature conditions (1200°C), the C, H, N, S/O elements in the sample generated CO_2, H_2O, N_2, SO_2/CO, and these different products were separated by adsorption-separation, and then quantified by a TCD detector to obtain the weight percentage of each element in the sample.

X-ray photoelectron spectra (XPS) was collected using ESCALAB-250Xi (Thermo Fisher Scientific).

Conclusion

We used iDPC-STEM imaging of Ca^{2+} ion exchanged FAU zeolite and ZTCs from those zeolites obtained at different growth times. Since the framework structure of FAU zeolite was atomically resolved, the carbon contrast in each channel can be directly identified with sub-nanometer resolution. The ZTC shows an ordered microporous structure with surface generated by extended network(s) composed of trivalently bonded carbon and with a high measured BET surface area. The hollow structure of ZTC was studied by gas adsorption and the inner and outer surfaces and volumes (S1, S2, V1, and V2) were identified from the fit pore distributions. Changes in the values and ratios of S1, S2, V1, and V2 helps one understand structure and structural evolution of ZTCs. iDPC-STEM imaging provided detailed information about the local structures, such as the distribution of carbons in FAU channels and about a thin carbon film that was at times found on the surface of the FAU particles; imaging of the C@FAU samples obtained at different growth times was used to study the structural evolution during the carbon deposition—as a function of the exposure time to acetylene under growth conditions. The carbon segments are non-uniformly distributed in each FAU channel at the initial stage and gradually connect to form a porous network that mostly (but not entirely) fills up the FAU framework. We suggest that this approach to studying the progression of carbon growth can guide in further understanding and perhaps modifying the local carbon structures in a variety of templates.

Acknowledgments

We thank Dr. Myoung Soo Lah and Dr. Tae Joo Shin for discussions. This work was supported by the Institute for Basic Science (IBS-R019-D1) of South Korea.

Author contributions

Conceptualization, M.A., B.S., G.Y., and R.S.R.; Methodology, M.A., G.Y, W.K.S., and R.S.R.; Investigation, M.A., B.S., X.C., H.X., K.D., A.F., C.V., G.Y., B.A., S.H.L., M.T., F.W. and R.S.R.; Resources, W.K.S. and R.S.R.; Writing – Original Draft, M.A., and B.S.; Writing – Review & Editing, M.A., B.S., X.C., H.X., K.D., A.F., C.V., S.H.L., W.K.S., M.T., F.W., and R.S.R.; Supervision, R.S.R.

References

1. Kroto, H.W., Heath, J.R., O'Brien, S.C., Curl, R.F., and Smalley, R.E. (1985). C60: Buckminsterfullerene. Nature *318*, 162-163. 10.1038/318162a0.

2. Iijima, S. (1991). Helical microtubules of graphitic carbon. Nature *354*, 56-58. 10.1038/354056a0.

3. Novoselov, K.S., Geim, A.K., Morozov, S.V., Jiang, D., Zhang, Y., Dubonos, S.V., Grigorieva, I.V., and Firsov, A.A. (2004). Electric field in atomically thin carbon films. Science *306*, 666-669. 10.1126/science.1102896.

4. Lenosky, T., Gonze, X., Teter, M., and Elser, V. (1992). Energetics of negatively curved graphitic carbon. Nature *355*, 333-335. 10.1038/355333a0.

5. Mackay, A.L., and Terrones, H. (1991). Diamond from graphite [7]. Nature *352*, 762. 10.1038/352762a0.

6. Phillips, R., Drabold, D.A., Lenosky, T., Adams, G.B., and Sankey, O.F. (1992). Electronic structure of schwarzite. Physical Review B *46*, 1941-1943. 10.1103/PhysRevB.46.1941.

7. Vanderbilt, D., and Tersoff, J. (1992). Negative-curvature fullerene analog of C60. Physical Review Letters *68*, 511-513. 10.1103/PhysRevLett.68.511.

8. Cao, X., Yin, Z., and Zhang, H. (2014). Three-dimensional graphene materials: Preparation, structures and application in supercapacitors. Energy and Environmental Science *7*, 1850-1865. 10.1039/c4ee00050a.

9. Han, S., Wu, D., Li, S., Zhang, F., and Feng, X. (2014). Porous graphene materials for advanced electrochemical energy storage and conversion devices. Advanced Materials *26*, 849-864. 10.1002/adma.201303115.

10. Huang, M.Z., Ching, W.Y., and Lenosky, T. (1993). Electronic properties of negative-curvature periodic graphitic carbon surfaces. Physical Review B *47*, 1593-1606. 10.1103/PhysRevB.47.1593.

11. Lee, H., Kim, K., Kang, S.H., Kwon, Y., Kim, J.H., Kwon, Y.K., Ryoo, R., and Park, J.Y. (2017). Extremely high electrical conductance of microporous 3D graphene-like zeolite-templated carbon framework. Scientific Reports *7*, 11460. 10.1038/s41598-017-11602-5.

12. Nishihara, H., and Kyotani, T. (2012). Templated nanocarbons for energy storage. Advanced Materials *24*, 4473-4498. 10.1002/adma.201201715.

13. Yang, Z., Xia, Y., and Mokaya, R. (2007). Enhanced hydrogen storage capacity of high surface area zeolite-like carbon materials. Journal of the American Chemical Society *129*, 1673-1679. 10.1021/ja067149g.

14. Zhou, J., Li, W., Zhang, Z., Wu, X., Xing, W., and Zhuo, S. (2013). Effect of cation nature of zeolite on carbon replicas and their electrochemical capacitance. Electrochimica Acta *89*, 763-770. 10.1016/j.electacta.2012.11.068.

15. Pun, S.H., and Miao, Q. (2018). Toward Negatively Curved Carbons. Accounts of Chemical Research *51*, 1630-1642. 10.1021/acs.accounts.8b00140.

16. Braun, E., Lee, Y., Moosavi, S.M., Barthel, S., Mercado, R., Baburin, I.A., Proserpio, D.M., and Smit, B. (2018). Generating carbon schwarzites via zeolite-templating. Proceedings of the National Academy of Sciences of the United States of America *115*, E8116-E8124. 10.1073/pnas.1805062115.

17. Hou, P.X., Yamazaki, T., Orikasa, H., and Kyotani, T. (2005). An easy method for the synthesis of ordered microporous carbons by the template technique. Carbon *43*, 2624-2627. 10.1016/j.carbon.2005.05.001.

18. Kim, K., Kwon, Y., Lee, T., Cho, S.J., and Ryoo, R. (2017). Facile large-scale synthesis of three-dimensional graphene-like ordered microporous carbon via ethylene carbonization in CaX zeolite template. Carbon *118*, 517-523. 10.1016/j.carbon.2017.03.082.

19. Kim, K., Lee, T., Kwon, Y., Seo, Y., Song, J., Park, J.K., Lee, H., Park, J.Y., Ihee, H., Cho, S.J., and Ryoo, R. (2016). Lanthanum-catalysed synthesis of microporous 3D graphene-like carbons in a zeolite template. Nature *535*, 131-135. 10.1038/nature18284.

20. Kyotani, T., Nagai, T., Inoue, S., and Tomita, A. (1997). Formation of New Type of Porous Carbon by Carbonization in Zeolite Nanochannels. Chemistry of Materials *9*, 609-615. 10.1021/cm960430h.

21. Lee, S.K., Park, H., Yoon, J.W., Kim, K., Cho, S.J., Maurin, G., Ryoo, R., and Chang, J.S. (2020). Microporous 3D Graphene-like Zeolite-Templated Carbons for Preferential Adsorption of Ethane. ACS Applied Materials and Interfaces *12*, 28484-28495. 10.1021/acsami.0c04228.

22. Ma, Z., Kyotani, T., and Tomita, A. (2002). Synthesis methods for preparing microporous carbons with a structural regularity of zeolite Y. Carbon *40*, 2367-2374. 10.1016/S0008-6223(02)00120-3.

23. Nishihara, H., Fujimoto, H., Itoi, H., Nomura, K., Tanaka, H., Miyahara, M.T., Bonnaud, P.A., Miura, R., Suzuki, A., Miyamoto, N., et al. (2018). Graphene-based ordered framework with a diverse range of carbon polygons formed in zeolite nanochannels. Carbon *129*, 854-862. 10.1016/j.carbon.2017.12.055.

24. Nishihara, H., Yang, Q.H., Hou, P.X., Unno, M., Yamauchi, S., Saito, R., Paredes, J.I., Martínez-Alonso, A., Tascón, J.M.D., Sato, Y., et al. (2009). A possible buckybowl-like structure of zeolite templated carbon. Carbon *47*, 1220-1230. 10.1016/j.carbon.2008.12.040.

25. Nueangnoraj, K., Nishihara, H., Imai, K., Itoi, H., Ishii, T., Kiguchi, M., Sato, Y., Terauchi, M., and Kyotani, T. (2013). Formation of crosslinked-fullerene-like framework as negative replica of zeolite y. Carbon *62*, 455-464. 10.1016/j.carbon.2013.06.033.

26. Baerlocher, C., Brouwer, D., Marler, B., and McCusker, L.B. Database of Zeolite Structures.

27. Chi, S., Kim, C., Lee, Y., and Choi, M. (2024). Diversity in Atomic Structures of Zeolite-Templated Carbons and the Consequences for Macroscopic Properties. JACS Au *4*, 1489-1499. 10.1021/jacsau.4c00028.

28. Aumond, T., Batonneau-Gener, I., Pouilloux, Y., Pinard, L., Wisser, D., Moreau, M., Vezin, H., Moissette, A., and Sachse, A. (2022). How do zeolite-templated carbons grow? Materials Today Chemistry *26*, 101053. 10.1016/j.mtchem.2022.101053.

29. Liu, Y., Wang, J., Serageldin, M.A., Wang, T., and Pan, W.P. (2021). Carbon deposition mechanism and structural changes for zeolite-templated carbons. Microporous and Mesoporous Materials *324*, 111311. 10.1016/j.micromeso.2021.111311.

30. Aumond, T., Esteves, M., Mocuta, C., Batonneau-Gener, I., Haines, J., Faccio, R., and Sachse, A. (2024). In situ X-Ray Powder Diffraction Investigation on the Development of Zeolite-Templated Carbons in FAU Zeolite. Chemistry-Methods *4*, e202400018. 10.1002/cmtd.202400018.

31. Cowley, J.M. (1976). Scanning transmission electron microscopy of thin specimens. Ultramicroscopy *2*, 3-16. 10.1016/S0304-3991(76)90161-3.

32. Erni, R., Rossell, M.D., Kisielowski, C., and Dahmen, U. (2009). Atomic-resolution imaging with a sub-50-pm electron probe. Physical Review Letters *102*, 096101. 10.1103/PhysRevLett.102.096101.

33. Haider, M., Uhlemann, S., Schwan, E., Rose, G., Kabius, B., and Urban, K. (1998). Electron microscopy image enhanced [7]. Nature *392*, 768-769. 10.1038/33823.

34. Lazić, I., and Bosch, E.G.T. (2017). Analytical Review of Direct Stem Imaging Techniques for Thin Samples. Advances in Imaging and Electron Physics.

35. Lazić, I., Bosch, E.G.T., and Lazar, S. (2016). Phase contrast STEM for thin samples: Integrated differential phase contrast. Ultramicroscopy *160*, 265-280. 10.1016/j.ultramic.2015.10.011.

36. Yücelen, E., Lazić, I., and Bosch, E.G.T. (2018). Phase contrast scanning transmission electron microscopy imaging of light and heavy atoms at the limit of contrast and resolution. Scientific Reports *8*, 2676. 10.1038/s41598-018-20377-2.

37. Liu, L., Wang, N., Zhu, C., Liu, X., Zhu, Y., Guo, P., Alfilfil, L., Dong, X., Zhang, D., and Han, Y. (2020). Direct Imaging of Atomically Dispersed Molybdenum that Enables Location of Aluminum in the Framework of Zeolite ZSM-5. Angewandte Chemie - International Edition *59*, 819-825. 10.1002/anie.201909834.

38. Shen, B., Chen, X., Cai, D., Xiong, H., Liu, X., Meng, C., Han, Y., and Wei, F. (2020). Atomic Spatial and Temporal Imaging of Local Structures and Light Elements inside Zeolite Frameworks. Advanced Materials *32*, 1906103. 10.1002/adma.201906103.

39. Shen, B., Chen, X., Fan, X., Xiong, H., Wang, H., Qian, W., Wang, Y., and Wei, F. (2021). Resolving atomic SAPO-34/18 intergrowth architectures for methanol conversion by identifying light atoms and bonds. Nature Communications *12*, 2212. 10.1038/s41467-021-22438-z.

40. Shen, B., Chen, X., Shen, K., Xiong, H., and Wei, F. (2020). Imaging the node-linker coordination in the bulk and local structures of metal-organic frameworks. Nature Communications *11*, 2692. 10.1038/s41467-020-16531-y.

41. Shen, B., Chen, X., Wang, H., Xiong, H., Bosch, E.G.T., Lazić, I., Cai, D., Qian, W., Jin, S., Liu, X., et al. (2021). A single-molecule van der Waals compass. Nature *592*, 541-544. 10.1038/s41586-021-03429-y.

42. Shen, B., Wang, H., Xiong, H., Chen, X., Bosch, E.G.T., Lazić, I., Qian, W., and Wei, F. (2022). Atomic imaging of zeolite-confined single molecules by electron microscopy. Nature *607*, 703-707. 10.1038/s41586-022-04876-x.

43. Yang, G., Liu, H., Arsakay, M., Shen, J., Shen, Y., Fatkhulloev, A., and Ruoff, R.S. (2023). A comprehensive parametric study of factors that influence synthesis of high-quality

ZTC using Ca2+ exchanged zeolite Y as the template. Carbon *215*, 118430. 10.1016/j.carbon.2023.118430.

44. Thommes, M., Kaneko, K., Neimark, A.V., Olivier, J.P., Rodriguez-Reinoso, F., Rouquerol, J., and Sing, K.S.W. (2015). Physisorption of gases, with special reference to the evaluation of surface area and pore size distribution (IUPAC Technical Report). Pure and Applied Chemistry *87*, 1051-1069. 10.1515/pac-2014-1117.

45. Gor, G.Y., Thommes, M., Cychosz, K.A., and Neimark, A.V. (2012). Quenched solid density functional theory method for characterization of mesoporous carbons by nitrogen adsorption. Carbon *50*, 1583-1590. 10.1016/j.carbon.2011.11.037.

46. Thommes, M., Cychosz, K.A., and Neimark, A.V. (2012). Chapter 4 - Advanced Physical Adsorption Characterization of Nanoporous Carbons. In Novel Carbon Adsorbents, J.M.D. Tascón, ed. (Elsevier), pp. 107-145. https://doi.org/10.1016/B978-0-08-097744-7.00004-1.

47. Nishihara, H., and Kyotani, T. (2018). Zeolite-templated carbons-three-dimensional microporous graphene frameworks. Chemical Communications *54*, 5648-5673. 10.1039/c8cc01932k.

48. Allen, L.J., D'Alfonso, A.J., and Findlay, S.D. (2015). Modelling the inelastic scattering of fast electrons. Ultramicroscopy *151*, 11-22. 10.1016/j.ultramic.2014.10.011.

49. Kirkland, E.J. (2010). Advanced computing in electron microscopy: Second edition 10.1007/978-1-4419-6533-2.